AGU PUBLICATIONS

JGR

Journal of Geophysical Research: Space Physics

RESEARCH ARTICLE
10.1002/2016JA023250

This article is a companion to *Sonnerup et al.* [2016] doi:10.1002/2016JA022362.

Key Points:
- Back-to-back switch-off shocks in magnetopause reconnection are examined by use of gyrotropic and pressure tensor models
- Normal heat fluxes are small, directed away from each shock. Total heat fluxes are larger, directed away from the reconnection site
- The CGL invariants show large anticorrelated variations and net entropy increases across each shock

Correspondence to:
B. Sonnerup,
Bengt.U.O.Sonnerup@dartmouth.edu

Citation:
Sonnerup, B., S. Haaland, G. Paschmann, T. Phan, and S. Eriksson (2016), Magnetopause reconnection layer bounded by switch-off shocks: Part 2. Pressure anisotropy, *J. Geophys. Res. Space Physics*, *121*, 9940–9955, doi:10.1002/2016JA023250.

Received 28 JUL 2016
Accepted 27 SEP 2016
Accepted article online 30 SEP 2016
Published online 28 OCT 2016

Magnetopause reconnection layer bounded by switch-off shocks: Part 2. Pressure anisotropy

Bengt Sonnerup[1], Stein Haaland[2,3], Götz Paschmann[4], Tai Phan[5], and Stefan Eriksson[6]

[1]Thayer School of Engineering, Dartmouth College, Hanover, New Hampshire, USA, [2]Max-Planck-Institut für Sonnensystemforschung, Göttingen, Germany, [3]Birkeland Centre for Space Science, University of Bergen, Bergen, Norway, [4]Max-Planck-Institut für extraterrestrische Physik, Garching, Germany, [5]Space Science Laboratory, University of California, Berkeley, California, USA, [6]Laboratory for Atmospheric and Space Physics, University of Colorado, Boulder, Colorado, USA

Abstract The jump conditions are analyzed in detail for two slow shocks bounding a reconnection plasma jet, observed on 3 August 2008 by the spacecraft THEMIS D (Time History of Events and Macroscale Interactions during Substorms) on the dayside, low-latitude magnetopause. Both shocks are near the switch-off limit. They have been previously examined by Sonnerup et al. (2016), on the basis of the simplest MHD version of the jump conditions. In the present paper, those conditions now include the pressure anisotropy, normal heat fluxes, and a finite normal magnetic field component, the effects of all of which are found to be small. We also present and discuss the, mostly field-aligned, measured total heat fluxes, which are found to be substantial and directed away from the reconnection site. We show that the double-adiabatic (Chew-Goldberger-Low) invariants are far from invariant. Their combination indicates a large entropy increase across the shock on the magnetospheric side with a much smaller increase across the shock on the magnetosheath side. The detailed cause of the entropy changes remains unclear but appears to involve irreversible transfer of energy between thermal motion parallel and perpendicular to the magnetic field. The new results confirm the previously found presence of heavy ions and the values of the effective ion mass on both sides of the event. They also confirm the need for an ion pressure correction in the shock on the magnetospheric side.

1. Introduction

In this paper, we continue to examine a magnetopause traversal by the spacecraft THEMIS D (Time History of Events and Macroscale Interactions during Substorms) (ThD), in which a reconnection jet was bounded by, or more precisely for the most part consisted of, two slow-mode shocks. Both shocks were near the switch-off condition, and the resulting symmetry, which is unusual at the magnetopause, was explained by the presence of heavy ions on the magnetospheric side of the event. Many other aspects of this event, including the presence of Hall electric fields, were discussed in what we will refer to as Paper 1 [*Sonnerup et al.*, 2016]. A schematic drawing of the event geometry and the spacecraft path through it is shown in Figure 1 of that paper. Other details and relevant references can also be found there. The analysis of the event was made complicated by two factors: first, the presence, on the magnetospheric side, of cold ions below the energy range of the plasma instrument but inferred from spacecraft charging and second, the presence of heavy ions that remained unidentified for lack of mass spectroscopy. The present study is based on data from the plasma spectrometer (ESA) [*McFadden et al.*, 2008] and the magnetometer experiment (FGM) [*Auster et al.*, 2008] on board the THEMIS spacecraft.

In Paper 1, we used the jump conditions in their simple one-dimensional MHD form as follows: mass conservation was used to calculate the, experimentally poorly determined, Alfvén-Mach number downstream of each shock (evaluated in the moving de Hoffmann-Teller (HT) frame, in which the convection electric field had been minimized); normal stress balance was used to establish the value of a multiplicative correction factor k_p for the ion pressure, needed in the shock on the magnetospheric side of the event (Shock 1) but not in the shock on the magnetosheath side (Shock 2); and tangential stress balance in the form of the switch-off condition was used to establish the need for, and value of, a quantity k_m amu, defining the effective ion mass in each shock. A value $k_m > 1$ is caused by the presence of heavy ions, some of them measured but unidentified by ESA and some below its energy range. They are presumably of ionospheric origin in Shock 1 and mostly solar wind He^{++} in Shock 2; the MHD energy balance, without heat loss, was used to show that the predicted

changes of plasma temperature and entropy across each shock agreed fairly well with the experimentally determined values. Because of the lack of information about the full particle population, especially for Shock 1, the jump conditions could not be checked in a strict sense, but they could be used to confirm that, with reasonable assumptions, the data could be made compatible with those conditions. The same statement applies to the present study, except as follows. The effects of pressure anisotropy are now included, and the energy equation is used to calculate the net heat flux into, or out of, each shock along the (x) direction normal to the magnetopause. Our new treatment also takes full account of all effects of the small, but finite, x component of the magnetic field, some of which had been neglected in Paper 1.

The THEMIS data include high-quality determinations of the ion and electron pressure tensors, albeit with a remaining uncertainty coming from the lack of ion mass discrimination. It is, at least partially, this feature that leads to the need for a multiplicative ion pressure correction factor k_p. The measured pressures were used in Paper 1 to investigate shock structure and possible dissipation mechanisms. The total pressures used were $p=(k_p p_i + p_e)$, where p_i and p_e are the measured ion and electron pressures and where $p_{i,e}=(p_{i,e\|}+2p_{i,e\perp})/3$. The ion pressure correction factor was found to be $k_p=1.27$ for Shock 1 and $k_p=1.00$ (i.e., no correction) for Shock 2. It was determined so as to satisfy the normal MHD pressure balance exactly. In the calculations it was assumed that unmeasured cold ion populations did not contribute to the pressures.

In section 2 of the present paper, we provide brief background information about the event, taken from Paper 1. In section 3, we reexamine the jump conditions by full inclusion of pressure anisotropy, both in the gyrotropic description and by direct use of the measured pressure tensor components. As before, we apply a multiplicative pressure correction k_p to the ion pressures $p_{i\perp}$ and $p_{i\|}$ or to the ion pressure tensor components, P_{ilm}, measured by the ESA instrument. We also use the total energy balance to quantitatively determine the net heat flux into or out of each shock, needed to conserve total energy. The jump conditions are first given in their general form, which is applicable to all shocks, and are then reduced to the form applicable to switch-off shocks (i.e., slow shocks in which the downstream tangential magnetic field is zero). In section 4, we discuss the calculated heat fluxes and compare them to values deduced from the distribution functions measured by ESA. In section 5, we examine the behavior of the "double-adiabatic (Chew-Goldberger-Low (CGL)) invariants" [*Chew et al.*, 1956] within each shock to see what information they can provide about the dissipation mechanisms and about the role of heat fluxes in the shocks. Section 6 contains a summary and further discussion of the results. Appendix A provides details about the k_p and k_m determinations. Appendix B contains details concerning the double-adiabatic theory and the associated entropy measure.

2. Basic Event Information

The magnetopause reconnection event of interest was described in detail in Paper 1. It was encountered by the spacecraft THEMIS D on 3 August 2008, in the time interval 16:58:56–17:01:05 UT. The event occurred on the dayside postnoon magnetopause at low southern latitude (the spacecraft location in GSM was $X=10.0$, $Y=2.1$, $Z=-3.8R_E$) under conditions of high magnetic shear (152°). An overview, taken from Paper 1, of various measured quantities is shown in Figure 1. In this figure, the number densities on the magnetosphere side (in Figure 1c on the left) were deduced from spacecraft charging up to the time where those densities start to agree with the ion density recorded by the ESA instrument. The corresponding temperatures have been calculated from the measured pressures by use of the corrected densities, as described in Paper 1. The first pair of vertical dashed/dash-dotted lines marks the upstream/downstream state of Shock 1, on the magnetospheric side of the event; the second pair of dash-dotted/dashed lines marks the downstream/upstream state of Shock 2, on the magnetosheath side. The southward directed reconnection jet is shown in Figure 1f. The measured parameter values upstream and downstream of each shock are given in Table 1, also taken from Paper 1, except for its bottom part, which contains information about the measured ion and electron pressure tensors. All magnetic field information in the table has been interpolated to the plasma time tags, and the plasma information is based on the usual, in our event incorrect, assumption that all ions are protons. The effects of the latter assumption are most pronounced in Shock 1, as can be seen from the unrealistically low upstream Mach numbers, $M_{A1}=V'_1/V_{A1}$ and $M^*_{A1}=V'_1/V^*_{A1}$, given in the table for this shock. Note that V' is the observed plasma speed, after transformation to the de Hoffmann-Teller (HT) frame, in which the upstream and downstream flows are, at least ideally, field aligned. The quantity $V_A=B/\left(\mu_0 N m_p\right)^{1/2}$ is the uncorrected Alfvén speed, and $V^*_A=(1-\alpha)^{1/2}V_A$ is the Alfvén speed corrected by the pressure anisotropy factor $\alpha=\left(p_{\|}-p_{\perp}\right)\mu_0/B^2$. Here N is the number density and m_p is the proton mass. The upstream Mach numbers in

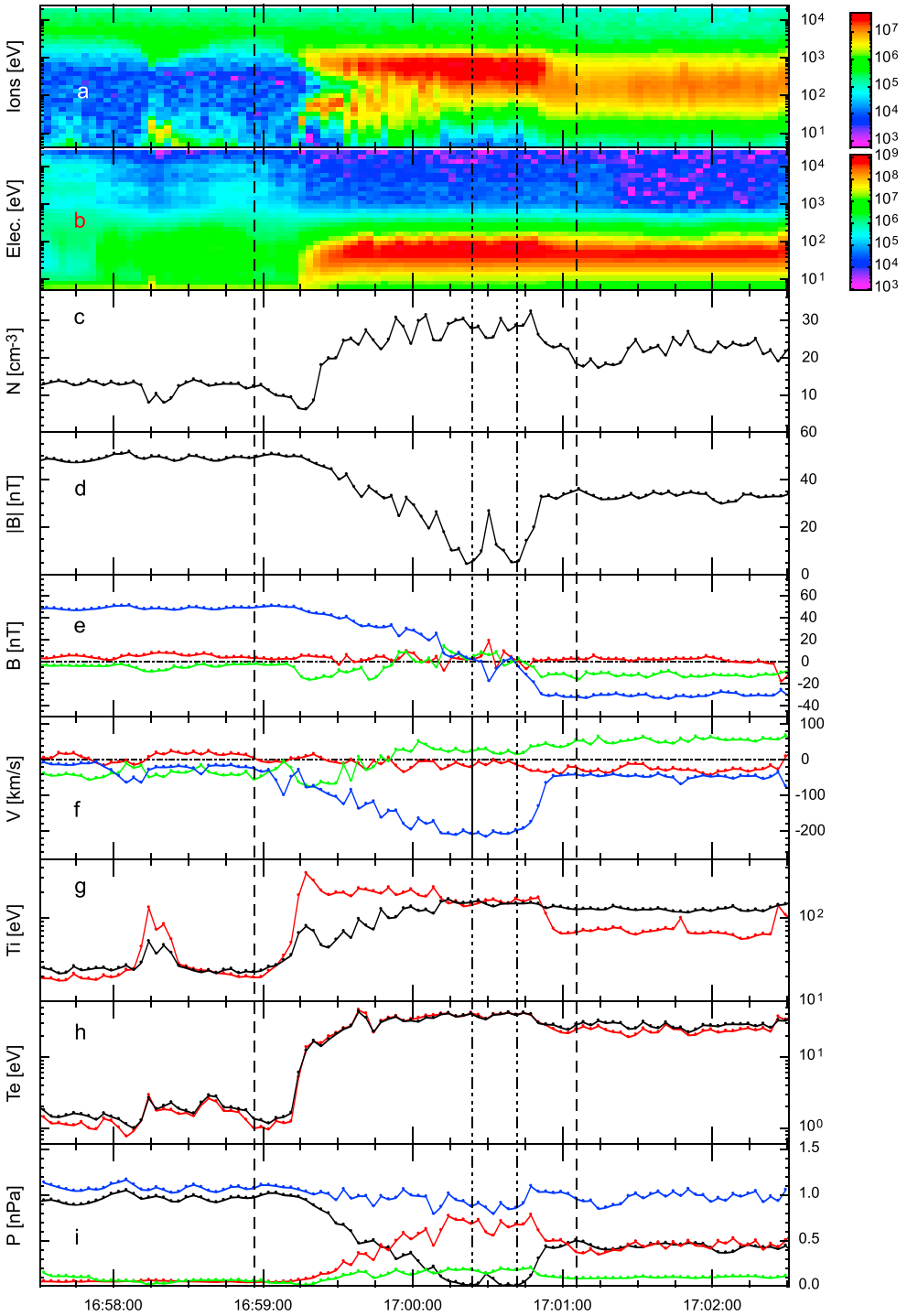

Figure 1. Overview of, 3 August 2008, magnetopause crossing by ThD (from Paper 1). Numbers are based on 3 s resolution plasma and magnetic field data: (a, b) Ion and electron energy-time spectrograms (color bar units are eV/cm^2 s). (c) Plasma number density. (d) Magnetic field magnitude. (e, f) Components of the magnetic field and of the plasma bulk velocity. (g) Ion temperatures (red: $T_{\|}$, black: $T_{\perp}$). (h) Same for electrons. (i) Magnetic pressures (black), ion (red), and electron (green) perpendicular pressures, sum of the pressures (blue). Vector quantities and tensors are in MVA coordinates (see Paper 1), with x (red; due sunward), y (green; due east), and z (blue; due north) along the minimum, intermediate, and maximum variance directions. Vertical lines mark the (dashed) upstream and (dash dotted) downstream reference times for the two shocks.

Journal of Geophysical Research: Space Physics

10.1002/2016JA023250

Table 1. Upstream and Downstream Reference Values for the Shocks[a]

	Shock 1		Shock 2	
	Upstream	Downstream	Downstream	Upstream
UT	16:58:56	17:00:23	17:00:41	17:01:05
N	12.33	27.81	28.51	18.45
B	[3.44,−1.97,49.27]	[2.38,3.65,2.63]	[1.58,1.28,−1.76]	[2.70,−15.30,−31.93]
V	[4.58,−56.63,−24.28]	[−21.59,23.20,−209.09]	[−13.96,15.08,−198.44]	[−20.74,53.64,−41.63]
V′	[18.72,−44.03,193.20]	[−7.44,35.79,8.39]	[0.19,27.67,19.05]	[−6.59,66.23,175.85]
$\mathbf{V}_A$	[21.36,−12.25,306.29]	[9.85,15.10,10.90]	[6.45,5.23,−y7.20]	[13.74,−77.77,−162.27]
α_i	−0.003115	−2.522344	16.385667	−0.175974
α_e	−0.000368	0.216435	0.223229	−0.011963
β_i	0.0451	59.5719	226.6987	0.7252
β_e	0.00265	16.76943	60.35502	0.16282
p_B	0.9720	0.0103	0.0029	0.5017
$p_{i\perp}$	0.0444	0.6814	0.6774	0.3734
$p_{e\perp}$	0.00268	0.18038	0.17630	0.08348
$p_{\|i}$	0.0383	0.6294	0.7716	0.1968
$p_{\|e}$	0.00196	0.18485	0.17759	0.07148
M_A^*	0.647	0.979	nan	0.956
M_A	0.648	1.780	3.056	1.042
P_i =	$\begin{bmatrix} 0.04391 & -0.000514 & 0.000572 \\ -0.000514 & 0.04500 & -0.002147 \\ -0.000572 & -0.002147 & 0.03811 \end{bmatrix}$	$\begin{bmatrix} 0.6357 & 0.02134 & -0.01328 \\ 0.02134 & 0.6294 & -0.04795 \\ -0.01328 & -0.04795 & 0.7269 \end{bmatrix}$	$\begin{bmatrix} 0.7336 & -0.002656 & -0.07246 \\ -0.002656 & 0.6730 & -0.007315 \\ -0.07246 & -0.007315 & 0.7195 \end{bmatrix}$	$\begin{bmatrix} 0.3633 & 0.003485 & 0.01575 \\ 0.003485 & 0.3426 & -0.07584 \\ 0.01575 & -0.07584 & 0.2376 \end{bmatrix}$
TrP_i	0.1270	1.9920	2.1261	0.9435
P_e =	$\begin{bmatrix} 0.00269 & -0.000110 & 0.000069 \\ -0.000110 & 0.00269 & -0.000110 \\ 0.000069 & -0.000110 & 0.001934 \end{bmatrix}$	$\begin{bmatrix} 0.18845 & 0.001028 & 0.008772 \\ 0.001028 & 0.18183 & -0.001951 \\ 0.008772 & -0.001951 & 0.17526 \end{bmatrix}$	$\begin{bmatrix} 0.1796 & 0.00184 & 0.00188 \\ 0.00184 & 0.1781 & -0.00265 \\ 0.00188 & -0.00265 & 0.1725 \end{bmatrix}$	$\begin{bmatrix} 0.08359 & -0.000892 & 0.002133 \\ -0.000892 & 0.08050 & -0.004926 \\ 0.002133 & -0.004926 & 0.07432 \end{bmatrix}$
TrP_e	0.00731	0.54555	0.5302	0.2384

[a]Densities N are in cm^{-3}; magnetic fields **B** (interpolated to the plasma time tags) are in nanotesla; velocities **V**, **V′** & $\mathbf{V}_A$ are in km/s; pressures p_B, $p_\perp$, $p_\parallel$, and the pressure tensor P are in nanopascal (nPa). Vector and tensor quantities are in MVA coordinates (for precise orientations, see Paper 1). Ion plasma data and Mach numbers in the table assume all particles to be protons. Velocities $\mathbf{V}' = \mathbf{V} - \mathbf{V}_{HT}$, as well as corresponding Mach numbers M_{A1}^* and M_{A1}, are in the de Hoffmann-Teller (HT) frame, with $\mathbf{V}_{HT}$ = (−14.1, −12.6, −217.5) km/s (see Paper 1). Table is taken from Paper 1, except for the measured ion and electron pressure tensor components and their traces. The high precision given for the data does not represent actual accuracy but is retained to permit detailed numerical checks.

the table are too small because, for a switch-off shock, they should be $M_{A1}=(1-\alpha_1)^{1/2}$ and $M^*_{A1}=1$. As discussed in Paper 1, the explanation for the discrepancy is that the effective ion mass must have been greater than the proton mass, which brings down the Alfvén speed and increases the Alfvén-Mach number. It can also influence the ion pressures. The downstream Mach numbers are ratios of small, fluctuating quantities; the values in the table are unreasonable for both shocks.

3. Jump Conditions

We now present details of the MHD jump conditions, associated with mass, momentum, and energy conservation. In what follows, upstream conditions for each shock will be denoted by the subscript 1 and downstream conditions by the subscript 2. The data used in the evaluation of these conditions are given in Table 1. In all equations, velocities $\mathbf{V}' \equiv \mathbf{V}-\mathbf{V}_{\rm HT}$ and associated Alfvén-Mach numbers $M_A=(V'/V_A)$ refer to the de Hoffmann-Teller frame, in which the flow is assumed to be steady and field aligned, upstream and downstream of (but not necessarily within) a planar 1-D shock. As in Paper 1, vector components given in the present paper are along the magnetic variance (MVA) axes (for details, see Paper 1), with the x axis pointing along the minimum variance direction, due sunward, the y axis pointing along the intermediate variance direction, due east, and the z axis pointing along the maximum variance direction, due north.

The mass density ρ should be based on the true effective ion mass, $k_m m_{\rm proton}$, which, for simplicity, we take to have a constant value across each shock. The pressure tensor P will be expressed, either in the gyrotropic approximation, i.e., $\mathrm{P}=p_\perp \mathrm{I}+\alpha\mathbf{BB}/\mu_0$, where α is the pressure anisotropy factor *Parks* [1991, p. 258] or by direct use of the measured pressure tensor components. In both descriptions the pressure contributions from both ions and electrons are included, the former corrected by a to-be-determined multiplicative factor k_p. The behavior of the two temperature components perpendicular to the magnetic field (see Figure A1d of Paper 1) indicates that the gyrotropic description should be adequate much of the time.

The normal component of the magnetic field, B_x, which should be strictly constant in a one-dimensional steady discontinuity, is in fact seen to have substantial variations during the event. In what follows, this field component will, for simplicity, be replaced by its average, $B_x = 3$ nT, as described in Paper 1.

3.1. Mass Balance

The mass conservation law is expressed as the jump condition $\rho_1 V'_{x1}=\rho_2 V'_{x2}$. When this expression is squared and divided by B_x^2/μ_0, it becomes $\rho_1 M^2_{Ax1}=\rho_2 M^2_{Ax2}$. The upstream and downstream flows in the HT frame are assumed field aligned so that $V'_x/B_x=V'/B$ and $M_{Ax}=M_A$. Therefore, mass conservation can be expressed as $\rho_1 M^2_{A1}=\rho_2 M^2_{A2}$. Because we assume the plasma composition to remain constant across each shock, we can write this in the same way as in Paper 1, namely,

$$N_1 M^2_{A1} = N_2 M^2_{A2} \tag{1}$$

As mentioned already, the downstream Mach numbers are unreliably determined from the measured plasma speeds and magnetic fields. They are ratios of two small numbers, both of which show considerable fluctuations in the measurements. For this reason, (1) will be used to evaluate M^2_{A2} from the corresponding upstream Mach number and the number density ratio. Where needed, this downstream Mach number will then be used in the remaining jump conditions.

3.2. Stress Balance

In terms of the total pressure tensor, i.e., the sum of the ion and electron parts, the normal and tangential stress balances can be expressed as

$$\left\{\left(M_A^2-1\right)B_x^2/\mu_0+\mathrm{P}_{xx}+B^2/2\mu_0\right\}_1^2=0 \tag{2}$$

$$\left\{\left(M_A^2-1\right)B_xB_z/\mu_0+\mathrm{P}_{xz}\right\}_1^2=0 \tag{3}$$

with an equation similar to (3) for the y component of the tangential stress balance. The "jump" notation $\{....\}_1^2 \equiv \{....\}_2-\{....\}_1$ signifies that the relation holds between the upstream (subscript 1) and the downstream (subscript 2) state of a shock (but not necessarily at points within the shock structure). Since the flow upstream and downstream, as seen in the HT frame, is assumed to be field aligned, we have expressed the normal and

tangential velocity components in that frame as $V'_{x,z} = M_A B_{x,z}/\sqrt{\mu_0 \rho}$. In these equations, we will also write $P_{xx} = k_p P_{ixx} + P_{exx}$ and $P_{xz} = k_p P_{ixz} + P_{exz}$, where k_p is an ion pressure correction factor to be determined so as to satisfy the normal stress balance exactly. We will also use $M_{A2}^2 = (N_1/N_2) M_{A1}^2$, taken from (1). If the upstream and downstream fields and pressure tensor components are taken directly from the measured data in Table 1 (where all ions are assumed to be protons), then (2) and (3) provide a pair of coupled linear equations for k_p and M_{A1}^2. Under ideal conditions, the y component of the tangential stress balance would then be identically satisfied. In the gyrotropic approximation, the same statements hold but now the pressure tensor terms are expressed as $P_{xx} = p_\perp + \alpha B_x^2/\mu_0$ and $P_{xz} = \alpha B_x B_z/\mu_0$.

For our event, the normal field component B_x does not remain strictly constant across each shock, presumably as a result of time variations or deviations from one-dimensional behavior. Also, the downstream field B_{z2} is fluctuating, which could be produced by the fire-hose instability and/or other effects. The result is that the value for M_{A1}^2 resulting from (2) and (3) comes out unreasonably low, which in turn leads to unreasonably high heat fluxes. For this reason, we will, as was done in Paper 1, replace the tangential stress balance, (3), by its switch-off version, obtained by putting $B_{z2} = 0$ and $P_{xz2} = 0$:

$$M_{A1}^2 - 1 = -P_{xz1}\mu_0/B_x B_{z1} = -\alpha_1 \tag{4}$$

Here the second equality follows from the fact that, in our event, the upstream state is very nearly gyrotropic so that we can write $P_{xz1} = \alpha_1 B_x B_{z1}/\mu_0$. Detailed formulas for the determination of the ion pressure correction factor k_p are provided in the first part of Appendix A.

Usually, magnetopause reconnection events are highly asymmetric and may involve slow shocks that are far from the switch-off state. For such events, use of (3) in its general form would be required and would give reliable results, provided B_x and B_{z2} were both accurately determined and stable.

3.3. Energy Balance

Once the ion pressure correction has been determined, one can then use the energy balance to find the net effective normal heat flux. In the equations to follow, it is assumed that all ion pressures have been corrected by the factor k_p and that the upstream Mach number is $M_{A1}^2 = 1 - \alpha_1$ with the ion part of α_1 corrected by k_p. The jump condition for total energy can then be written as

$$\left\{\rho V'_x \left(V'^2/2 + Tr\,\mathrm{P}/(2\rho) + \hat{\mathbf{x}} \cdot \mathrm{P} \cdot \mathbf{V}'\right) + q_x\right\}_1^2 = 0 \tag{5}$$

Here we recognize $V'^2/2$ and the pressure tensor trace $Tr\mathrm{P}/(2\rho)$ as the kinetic and internal energy per unit mass; the term $\hat{\mathbf{x}} \cdot \mathrm{P} \cdot \mathbf{V}'$ represents the rate of work done by all pressure forces. The Poynting vector $\mathbf{S}$ is absent since it has no x component, but the x component of the heat flow vector $\mathbf{q}$ can potentially contribute and will appear in our results as a net change $\Delta q_x = (q_{x2} - q_{x1})$ across each shock. This change represents the result deduced from the energy balance.

Upstream and downstream, the flow in the HT frame is field aligned so that we may write

$$\hat{\mathbf{x}} \cdot \mathrm{P} \cdot \mathbf{V}' = P_{xx} V'_x + P_{xy} V'_y + P_{xz} V'_z = \left(V'_x/B_x\right)\left(P_{xx} B_x + P_{xy} B_y + P_{xz} B_z\right) \tag{6}$$

We also have $V'^2/2 = M_A^2 B^2/2\mu_0\rho$. By use of (6), equation (5) then becomes

$$\left\{\left[M_A^2 B_2^2/\mu_0 + Tr\,\mathrm{P}/2 + \left(P_{xx} B_x + P_{xy} B_y + P_{xz} B_z\right)/B_x\right]/\rho + q_x/\rho V'_x\right\}_1^2 = 0 \tag{7}$$

In (7) we can, as before, express M_{A2} in terms of M_{A1} by use of (1).

In the gyrotropic approximation, we again replace the pressure tensor components in (6) and (7) by $P_{xx} = p_\perp + \alpha B_x^2/\mu_0$, $P_{xy} = \alpha B_x B_y/\mu_0$, $P_{xz} = \alpha B_x B_z/\mu_0$, and also $Tr\mathrm{P} = 2p_\perp + p_{||}$.

Detailed formulas for the energy balance are given in the second part of Appendix A.

3.4. Results From The Shock Jump Conditions

The results from the jump conditions are given in Table 2. We first compare the correction factors for ion pressure and ion mass to those obtained from the simplified analysis in Paper 1, namely, $k_p = 1.27$ and a nominal

Table 2. Results From the Shock Jump Conditions[a]

Corrected Quantities	Shock 1	Shock 2
Upstream normal field B_x (nT)	3.00	3.00
Measured field ratio B_{z2}/B_{z1}	0.0534	0.0551
Magnetic pressure $B_1^2/2\mu_0$ (nPa)	0.9720	0.5017
Gyrotropic description		
Ion pressure correction k_p	1.2705	0.9637
Mach number M_{A1}	1.0022	1.0870
Mach number M_{A2}	0.6672	0.8744
Mass correction k_m	2.3918	1.0882
Heat flux factor $\Delta q_x/V'_{x1}$ (nPa)	−0.0091	−0.0043
Net heat flux Δq_x (mW/m^2)	$-0.1099 \cdot 10^{-3}$	$+0.0683 \cdot 10^{-3}$
Pressure tensor description		
Ion pressure correction k_p	1.3179	1.0960
Mach number M_{A1}	1.0022	1.0976
Mach number M_{A2}	0.6673	0.8830
Mass correction k_m	2.3921	1.1097
Heat flux factor $\Delta q_x/V'_{x1}$ (nPa)	−0.0554	−0.0915
Net heat flux Δq_x (mW/m^2)	$-0.6692 \cdot 10^{-3}$	$+1.4535 \cdot 10^{-3}$

[a]Switch-off condition, $B_{z2} = 0$, is used, along with the ion pressure correction factor, k_p. The nominal mass correction factor, k_m, is evaluated under the assumption that the correction factor for velocity is k_v=1, which may in reality not be precisely true; the nominal mass corrections actually represent the product $k_v^2 k_m$, with k_v for Shock 1 in the allowable range 0.98–1.30, as discussed in Paper 1. Net heat fluxes Δq_x are calculated from the heat flux factors by multiplication by $V'_{x1} = \pm|V'_1|B_x/|B_1|$, with $B_x = 3$ nT.

value (i.e., assuming $k_v = 1$) of the mass correction factor $k_m = 2.39$ for Shock 1 and $k_p = 1.00$ and $k_m = 1.09$ for Shock 2. Table 2 shows very good agreement with those numbers for the gyrotropic model, with somewhat larger (unexplained) deviations of the numbers from the pressure tensor approach. These discrepancies serve as an indicator of the uncertainties in the pressure correction factors. Note that the mass and pressure correction factors seem to go together: they are both substantially larger than 1 in Shock 1 and both close to 1 in Shock 2. This behavior is consistent with the conclusion that these corrections are, at least in part, the direct or indirect result of the presence, in Shock 1, of substantial amounts of unidentified heavy ions, some of which fall below the low energy cutoff of the ESA instrument in the early upstream part, but are visible in most of the remaining part, of the shock. As already noted in Paper 1, the low energy ESA cutoff and other effects may possibly also lead to the need for a correction factor k_v of the field-aligned ion velocity at the upstream station of Shock 1. For both shocks, errors in $\mathbf{V}_{HT}$ could also lead to $k_v \neq 1$.

The response of an ion spectrometer without mass discrimination to inputs consisting of a mixture of protons and heavier ions is complicated [see, e.g., *Paschmann et al.*, 1986]. Number densities, velocities, and pressure tensors are all affected, and their true values cannot be uniquely deduced from the measurements. However, from the formulas in *Paschmann et al.* [1986] one can show that the measured pressure tensor component P_{xx} is always underestimated in a mixture of protons and heavier ions. The result is the need for an ion pressure correction factor $k_p > 1$, although it is doubtful that this effect can be large enough to explain the k_p values we have deduced. Time dependence and deviations from our simple wedge-shaped shock configuration may also play important roles. We note that, at the downstream reference point of Shock 1, it is the pressure component P_{xx} that provides the main force balancing the upstream magnetic pressure. It is mainly a defect in this term that creates the need for the ion pressure correction. This pressure component also enters into the energy balance in an important way.

4. Heat Fluxes

In Paper 1, the net heat flux out of, or into, each shock was assumed to be zero. This assumption is supported by the small heat flux factors given in Table 2, at least for the gyrotropic description. In the pressure tensor description they are somewhat larger but still reasonably small. The heat flux factors given in Table 2 have the physical dimension of nanopascal (nPa) and are seen to be small compared to the upstream magnetic pressure $p_B = {B_1}^2/(2\mu_0)$ (given in row 3 of the table), the latter being one of the larger terms in the energy balance and being of order 1 nPa for Shock 1. With an assumed upstream normal plasma speed, $V'_{x1} = \pm B_x|V'_1|/|B_1|$, with $B_x = +3$ nT, the heat flux factors convert to the net heat fluxes given in Table 2; they do not exceed $\Delta q_x = \pm 1.5 \cdot 10^{-3}$ mW/m^2. Assuming the total heat flux vectors to be approximately field aligned, their full magnitudes at the upstream reference times would be some 10 times larger, i.e., they would be about $|\mathbf{q}| = 1.5 \cdot 10^{-2}$ mW/m^2 or less.

In light of the extensive calculations needed to determine the normal heat fluxes from energy conservation (see Appendix A), it is impressive that they come out as small as they do. Also, the fact that the signs of the heat flux factors in Table 2 are consistent and negative for the two different descriptions suggests that, while small, they could possibly be significantly different from zero, representing a small net heat flux away from the magnetopause layer for both shocks, as indicated by the values of Δq_x in Table 2 (remember that V'_x is positive for Shock 1 and negative for Shock 2).The estimates of the separatrix locations given in Paper 1 indicate that the upstream station for each shock was located well downstream of the corresponding separatrix. This means that, for both shocks, the upstream station was magnetically connected to some point on the shock, located closer to the magnetic *X* point. Any heat flux escaping from the shock along the magnetic field on the two sides of the magnetopause should therefore have been observable at our upstream stations. Since they were small, we conclude that, locally, heat flux away from (or into) these shocks did not play a major role in the overall energy balance. But we cannot conclude that they were precisely zero, as we will show below.

The THEMIS plasma instruments delivered 3-D ion and electron distribution functions of sufficient quality to permit a meaningful determination of heat flux vectors from the appropriate third moment of the distribution function (see, e.g., *Paschmann et al.* [1998, equation (6.8)] after subtraction of a missing term, $(\rho/2)\mathbf{V}V^2$). The results for our event are shown in Figure 2. The heat flux vectors are shown separately for ions and electrons in Figures 2d and 2e, in terms of their components along the MVA axes. The normal (x) components (red curves) are indeed small, especially at the upstream reference times of the two shocks, and appear to fluctuate around zero. Within measurement errors, they would be consistent with the near-zero net normal heat flux predicted from the shock jump conditions. Note that the latter fluxes are too small to show up on the heat flow scales used in Figure 2. In that figure, one can see that there are substantial ion heat fluxes tangential to the magnetopause within each shock (except in the short interval between the two shocks), as well as in the magnetosheath. These fluxes are directed southward, i.e., away from the reconnection site, in both shocks as well as in the magnetosheath. Within errors, they could be consistent with the presence of a small net heat flux away from the magnetopause (indicated by the negative sign of $\Delta q_x/V'_x$ in Table 2). The tangential electron heat fluxes are generally small, except for a 20 s southward pulse around the upstream reference time for Shock 2. The tangential ion and electron heat fluxes seen in the magnetosheath could plausibly originate in Shock 2 at locations closer to the reconnection site. On the magnetospheric side, we note that the precursor density depression (centered at 16:58:15; see Figure 2b) upstream of Shock 1 and associated magnetic structure (Figure 1) shows an ion heat flux signature (Figure 2d) consistent with a brief entry into the rotational discontinuity (RD) at the upstream edge of Shock 1, as mentioned already in Paper 1. We also note that it is at the beginning of the RD, at 19:59:10 UT, that the large field-aligned heat flux in Shock 1 begins to develop.

Figures 2f–2h show the components of the ion (black) and electron (red) heat fluxes perpendicular and parallel to the magnetic field, along with the angle between the heat flux and magnetic vectors, with angles 0° and 180° indicating flux parallel and antiparallel to **B**. For both ions and electrons, the former angle dominates in Shock 2, the latter in Shock 1, although the fluctuations are substantial, especially for the electrons. The conclusion is that, throughout most of the magnetopause, there is a substantial heat flux directed away from the reconnection site.

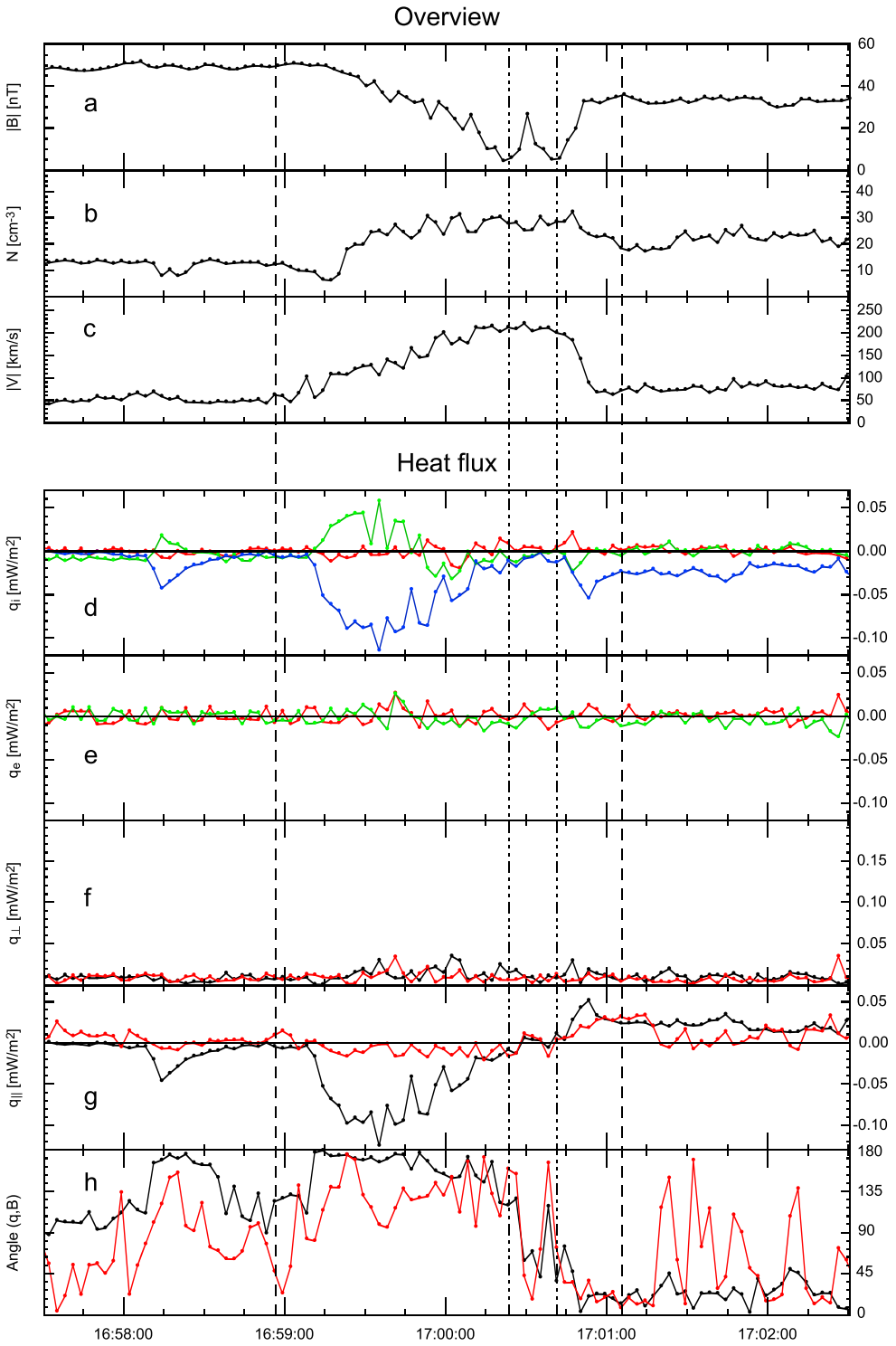

Figure 2. Heat flux vectors, **q**, for ions and electrons, calculated from measured distribution functions. (a–c) Overview values of field magnitude (nT), number density (cm^{-3}), and flow speed in the spacecraft frame (km/s). (d, e) MVA components (*x*, red; *y*, green; and *z*, black) of measured heat fluxes (mW/m^2), $\mathbf{q}_i$ for ions, and $\mathbf{q}_e$ for electrons (same color code). (f–h) Components of ion (black) and electron (red) heat fluxes, perpendicular and parallel to **B**, and the angle α between **q** and **B** ($\alpha = 0°$ for parallel and $\alpha = 180°$ for antiparallel orientations). No correction factors for pressure, velocity, or effective ion mass are included in the figure.

5. Double-Adiabatic Invariants

The Chew-Goldberger-Low (CGL) adiabatic invariants [*Chew et al.*, 1956] are defined by

$$C_{\parallel} = \kappa_b T_{\parallel} B^2 / N^2 \tag{8}$$

$$C_{\perp} = \kappa_b T_{\perp} / B \tag{9}$$

As demonstrated in Appendix B, conservation of total energy, after subtraction of the mechanical part, together with certain important assumptions, leads to the following relation between the spatial derivatives of the two invariants

$$(1/2)\kappa_b T_{\parallel}(\mathrm{d}/\mathrm{d}x) \ln C_{\parallel} + \kappa_b T_{\perp}(\mathrm{d}/\mathrm{d}x) \ln C_{\perp} + \left(1/\left(2NV_x'\right)\right) \mathrm{d}q_x/\mathrm{d}x = 0 \tag{10}$$

Here κ_b is Boltzmann's constant and V_x' is the normal (x) component of the plasma flow velocity, evaluated in the HT frame. Note again that V_x' is positive in Shock 1 and negative in Shock 2. Also, q_x represents an effective heat flux along the magnetopause normal, required to conserve total energy. The total heat flux vector is expected to be approximately parallel or antiparallel to the magnetic field, as is indeed, albeit very approximately, the case in Figure 2. This effective heat flux may not be a true heat flux but could instead be partially, or even wholly, associated with effects such as viscous or resistive dissipation or with a localized electric field component E_x', not included in the energy equation we used. In deriving (10), it was simply assumed that $\mathbf{E} + \mathbf{V} \times \mathbf{B} = 0$ (see Appendix B).

As in Figures 3d–3f, the two adiabatic invariants, their name notwithstanding, in fact undergo large variations in the event. This should not come as a surprise: their invariance places severe restrictions on the heat flux tensor [*Chew et al.*, 1956], which are unlikely to be met in our event, where large field-aligned heat fluxes are present (see Figure 2) within the exhaust jet.

As a consequence of the density minimum at the beginning of Shock 1, both invariants show a pronounced maximum at that location. Elsewhere, the variations are anticorrelated, mainly as a consequence of their opposite dependence on the field strength B. The entropy parameter, derived in Appendix B and shown in the third panel of this set, has a large increase across Shock 1 and a much smaller increase across Shock 2. There is also a large entropy maximum at the location of the density minimum.

To evaluate the space derivatives in (10) from the observed time derivatives, we note that they are proportional, $\mathrm{d}/\mathrm{d}t = -V_{\mathrm{mpx}}\mathrm{d}/\mathrm{d}x$, where V_{mpx} is the local magnetopause speed, which is negative (−14.1 km/s; see explanatory notes for Table 1) on average in the event, but where brief positive excursions may have occurred.

Except for distortions caused by a nonconstant value of the magnetopause speed V_{mpx}, Figures 3g–3i show the behavior of the first two terms on the right-hand side of (10) and also their sum. The latter shows that the sum is approximately zero during most of the event. This result is consistent with the conclusion that the combined effects of physical normal heat fluxes (see section 4), resistive, and viscous dissipation (see Paper 1) are for the most part not important in the shock structures. An exception is the large bipolar pulse associated with the density depression at the beginning of Shock 1. This pulse is produced mainly by a strong bipolar pulse in the parallel term (Term 1). If interpreted in terms of a normal heat flux, q_x, the implication would be an earthward heat flux followed by a sunward heat flux, making the density depression (which is accompanied by a maximum in both $T_{\parallel}$ and $T_{\perp}$) (see Figure 3c) a source of the heat flux. Note that similar, but smaller, bipolar pulses in Terms 1 and 2 are present also in the early partial entry (at 16:58:15 UT) into the RD associated with Shock 1.

As mentioned already, the interpretation of q_x in terms of a true heat flux need not be entirely appropriate. Any deviations from the model assumptions that led to (10) could be responsible for all or parts of the q_x term in that equation. In particular, it was shown in Paper 1 that a substantial Hall electric field is associated with the density minimum; the effects of such a field are not explicitly included in (10). The Hall electric field itself does not lead to dissipation because it is perpendicular to the current. But, as argued in Paper 1, it breaks the frozen condition for the ions, which leads to a violation of the assumption of field-aligned ion flow, on which (10) is based.

In Paper 1, it was also shown that a small rotation of the tangential magnetic field accompanied the density minimum, with the associated in-plane current forming part of a Hall current loop. It was concluded that the

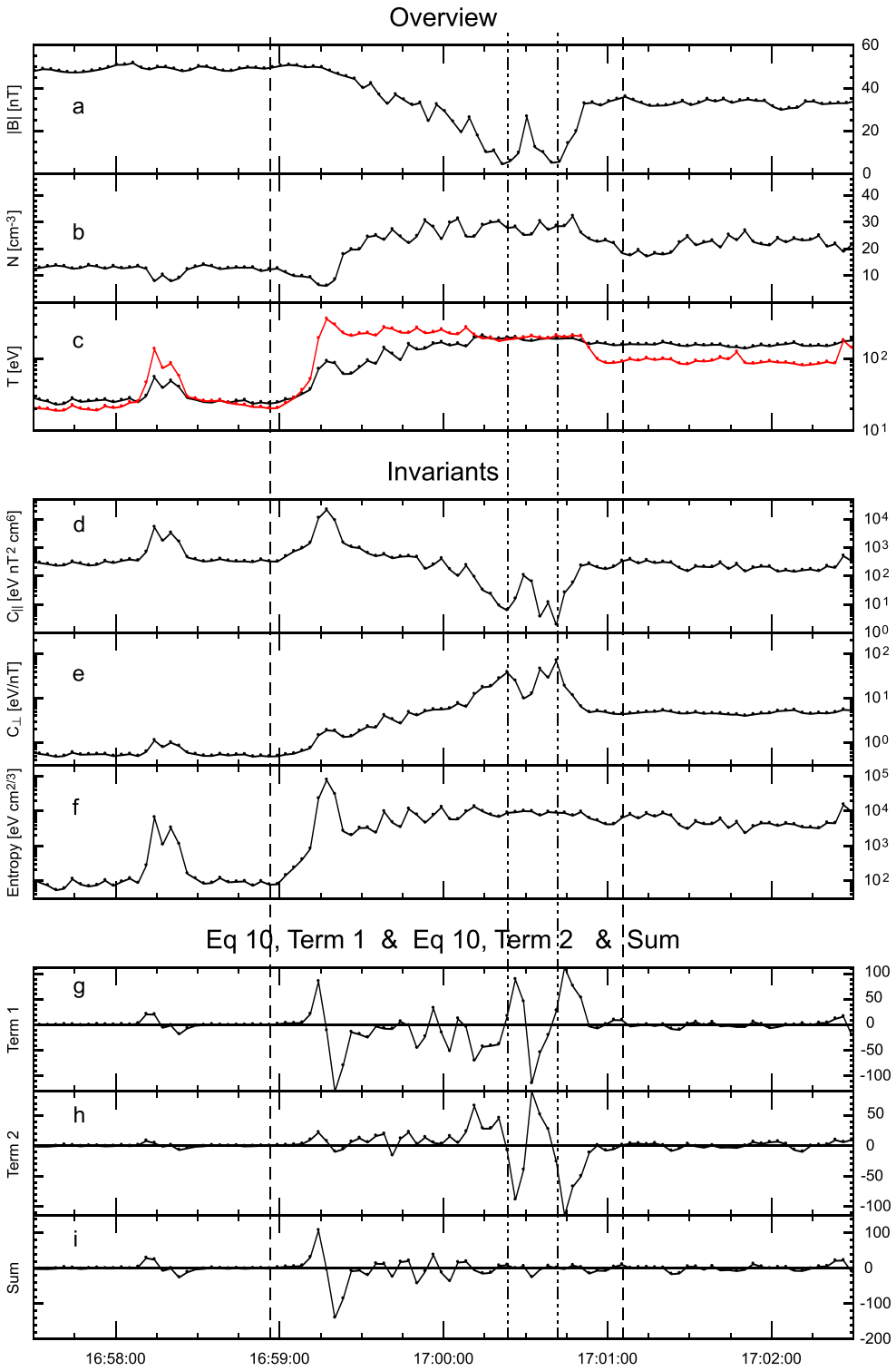

Figure 3. Time series of the double-adiabatic invariants $C_{\parallel}$ and $C_{\perp}$ of the entropy and of the main terms in equation (10). (a–c) Time series of field magnitude, number density, and combined (ion + electron) plasma temperatures, with $T_{\parallel}$ in red and $T_{\perp}$ in black. (d–f) Behavior of $C_{\parallel}$ (eV nT^2 cm^6), $C_{\perp}$ (eV/nT), and the entropy measure $C_{\parallel}^{1/3}C_{\perp}^{2/3}=\kappa_b T_{\parallel}^{1/3}T_{\perp}^{2/3}/N^{2/3}$ (eV cm$^{2/3}$); see Appendix B; (g–i) Terms 1 and 2 on the right-hand side of equation (10), with the space derivatives converted to time derivatives, using $V_{HTx} = -14.1$ km/s. The temperatures used in $C_{\parallel}$ and $C_{\perp}$ do not include the ion pressure correction factor k_p.

flow in this structure must have been Alfvénic; it was interpreted as a rotational discontinuity (RD) attached to the upstream edge of Shock 1, which is its expected location relative to a switch-off shock. It was further shown that Shock 2 also had such a leading edge RD, albeit a much less pronounced one.

6. Summary and Discussion

The present paper is a sequel to Paper 1 [*Sonnerup et al.*, 2016], in which the general features were described of an unusual magnetopause reconnection event, in which the exhaust jet was bounded by (and consisted of) back-to-back switch-off shocks. Included in the analysis was a simplified version of the shock jump conditions in which pressure anisotropy was not included (except to specify the upstream Alfvén-Mach numbers). In the follow-up study presented here, pressure anisotropy is included, either by use of the gyrotropic description or by direct use of the measured pressure tensor components. Also, the behavior of the CGL adiabatic invariants was examined. The following results were obtained:

1. Inclusion of pressure anisotropy in the shock jump conditions gave results consistent with the findings in Paper 1. Specifically, the ion pressure correction factor required for Shock 1 (on the magnetospheric side) in Paper 1 came out nearly the same ($k_p = 1.27$) in the gyrotropic description but, for unknown reasons, somewhat larger ($k_p = 1.32$) in the pressure tensor description. For Shock 2 (on the magnetosheath side), the value used in Paper 1 was $k_p = 1$. Here the gyrotropic description gave $k_p = 0.96$ and the pressure tensor method gave $k_p = 1.10$. These deviations are indicative of the overall uncertainties in the calculated k_p values.
2. The nominal effective ion masses deduced are in good agreement with those given in Paper 1 ($k_m = 2.39$ amu for Shock 1 and $k_m = 1.09$ amu for Shock 2), suggesting a significant presence of what is probably ionospheric O^+ (9.3%) in Shock 1 and a small amount of what is probably He^{++} (3.0%) of solar wind origin in Shock 2.
3. The net heat flux in the normal direction for each shock was assumed to be zero in Paper 1. In the gyrotropic model of the energy conservation law, this heat flux component did indeed come out very small, with somewhat larger,but still small values resulting from the directly measured pressure tensors. The net normal heat flux was directed away from the magnetopause in both descriptions and for both shocks.
4. Within the two shocks, there were substantial, field-aligned heat fluxes. These fluxes were approximately antiparallel to the magnetic field in Shock 1 and approximately parallel to the field in Shock 2. Since the spacecraft was located well south of the reconnection site, this behavior indicates that the heat fluxes were directed away from this site in both shocks. However, one should not conclude that they were generated at the reconnection site itself. It appears likely that they originated within the two shocks, throughout the region between the reconnection site and the spacecraft.
5. The CGL adiabatic invariants were not invariant in the event, a not surprising result, given the restrictive conditions under which their constancy was derived [*Chew et al.*, 1956]. As seen by an observer riding with the plasma flow from each of the two upstream regions into the exhaust jet, the longitudinal invariant, $C_{\|}$, decreased and the transverse invariant, $C_{\perp}$, increased, as did the entropy, across both shocks,. This result is noteworthy, especially for the transverse invariant, which is often thought to represent the conservation of magnetic moment. In both shocks, irreversible transfer must occur from energy associated with parallel, to energy associated with perpendicular, thermal motion. This effect could be, at least partially, the result of the intermixing of two particle populations in the exhaust: magnetospheric ions moving sunward and magnetosheath ions moving earthward.
6. In the magnetosphere, upstream of Shock 1, the temperatures and the plasma β values were both very small, with $T_{\perp} > T_{\|}$. Upstream of Shock 2 (in the magnetosheath) the same sense of the anisotropy was present but now with substantial temperatures and plasma β values of order 1. In the center of the exhaust, the temperature was nearly isotropic. We note that the changes in $T_{\|}$ were much more abrupt than those in $T_{\perp}$ and that, for both shocks, those rapid changes occurred slightly upstream of the shock structure proper. It is our conclusion that this behavior was caused by Hall electric field structures just upstream of Shock 1 and probably also of Shock 2. These electric fields are directed toward the center of the event. They cause the frozen in-field condition for ions to be broken, thereby allowing the speed at the center of the exhaust jet to be less than that predicted by simple MHD.
7. The presence of intrinsic normal electric fields could be deduced directly from the measurements but only for Shock 1 (see Paper 1). In this shock, it was seen to coincide with a number density minimum and a magnetic field rotation, the latter presumably generated by a portion of an in-plane Hall current loop. For Shock 2, the presence of an intrinsic normal electric field could not be established, since reliable

measurements of the total electric field became unavailable in the middle of the event. But a slight upstream magnetic field rotation was seen for this shock, coincident with the abrupt change in $T_{\|}$ (see Paper 1). The more gradual increases in $T_{\perp}$ were smaller and coincided with the magnetic field changes. From the abrupt upstream changes of $T_{\|}$, it appears that the overall shock structures depend in an important way on Hall-induced structures immediately upstream of each shock.

Appendix A: Pressure Correction Factor

A1. Gyrotropic Description

In the gyrotropic approximation, we can write $P_{xx} = p_{\perp} + \alpha B_x^2/\mu_0$ and $P_{xz} = \alpha B_x B_z/\mu_0$ so that the normal and tangential components of the stress balance become

$$M_{A1}^2(1 - N_1/N_2)B_x^2/\mu_0 = \left[\left(p_{\perp 2} - p_{\perp 1}\right) + \left(p_{B2} - p_{B1}\right) + \left(\alpha_2 - \alpha_1\right) B_x^2/\mu_0 \right. \tag{A1}$$

$$M_{A1}^2 - 1 + \alpha_1 = 0 \tag{A2}$$

In the pair (A1) and (A2), we now correct all ion pressures by the unknown correction factor k_p so that $p_{\perp} = k_p p_{i\perp} + p_{e\perp}$, $p_{\|} = k_p p_{i\|} + p_{e\|}$, and $\alpha = k_p \alpha_i + \alpha_e$. The result from (A1) is the following expression for k_p:

$$k_p = \left(A_a + A_b + A_c\right)/A_d \tag{A3}$$

where

$$\begin{aligned} A_a &= p_{B1} - p_{B2} \\ A_b &= p_{e1\perp} - p_{e2\perp} \\ A_c &= \left(B_x^2/\mu_0\right)\left[\left(1 - \alpha_{e2}\right) - \left(N_1/N_2\right)\left(1 - \alpha_{e1}\right)\right] \\ A_d &= \left(p_{i2\perp} - p_{i1\perp}\right) + \left(B_x^2/\mu_0\right)\left[\left(\alpha_{i2}\right) - \left(N_1/N_2\right)\alpha_{i1}\right] \end{aligned}$$

Once k_p has been obtained from (A3), one then obtains

$$M_{A1}^2 = 1 - k_p \alpha_{i1} - \alpha_{e1} \tag{A4}$$

where $\alpha i1$ and α_{e1} are taken from Table 1. From the resulting value of M_{A1}^2 we can then obtain the effective mass from the uncorrected M_{A1}^2 values in Table 1:

$$k_m k_v^2 = M_{A1}^2 / \left(M_{A1}^2\right)_{\text{Table1}} \tag{A5}$$

Here the effective mass ratio is $k_m = m_{\text{effective}}/m_{\text{proton}}$ and k_v is a multiplicative correction factor for the measured plasma speed in the HT frame, with a possible range of values $0.98 < k_v < 1.30$ for Shock 1, as discussed in Paper 1. The "nominal" value of k_m corresponds to the choice $k_v = 1$.

The gyrotropic version of the total energy balance (7) can be written as

$$\Delta q_x/V'_{x1} = H_1 - \left(N_1/N_2\right) H_2 \tag{A6}$$

where H, the total enthalpy per unit volume, is

$$H = M_A^2 p_B + 3p_{\|}/2 + p_{\perp} \tag{A7}$$

The information needed in the above calculations is given in Table 1. Note that the ion pressures in (A7) are the ones obtained after correction by the factor k_p and that the M_A values are those given in Table 2. The resulting net heat flux factors are also in the latter table.

A2. Pressure Tensor Description

The situation for this description is similar. We again use (1) to eliminate M_{A2}^2 in terms of M_{A1}^2. Using the pressure correction k_p, we also write $P_{xx} = k_p P_{ixx} + P_{exx}$, $P_{xy} = k_p P_{ixy} + P_{exy}$, and $P_{xz} = k_p P_{ixz} + P_{exz}$.

Since the upstream state is closely gyrotropic, we also have $P_{xz1}=\alpha_1 B_x B_{z1}/\mu_0$, which means that the gyrotropic switch-off condition, $M_{A1}^2=1-\alpha_1$, is recovered. The normal stress balance (2) gives

$$\left[1-\left(k_p P_{ixz1}+P_{exz1}\right)\mu_0/B_x B_{z1}\right]\left(1-N_1/N_2\right)B_x^2/B_1^2-k_p\left(P_{ixx2}-P_{ixx1}\right)\mu_0/B_1^2=\left(P_{exx2}-P_{exx1}\right)\mu_0/B_1^2-\left(1-B_2^2/B_1^2\right)/2 \tag{A8}$$

The resulting expression for k_p is of the same form as (A3) but now with different definitions of three of the four terms A_a to A_d:

$$\begin{aligned} A_a &= p_{B1}-p_{B2} \\ A_b &= P_{exx1}-P_{exx2} \\ A_c &= \left(B_x^2/\mu_0\right)\left(1-\left(N_1/N_2\right)\right)\left(1-\alpha_{e1}\right) \\ A_d &= \left(B_x^2/\mu_0\right)\left(1-\left(N_1/N_2\right)\right)\alpha_{i1}\right)-P_{ixx1}+P_{ixx2} \end{aligned}$$

The evaluation of M_{A1}^2 and k_m is again made from (A4) and (A5).

The total energy balance is, as before, expressed by (A6) but now with a different expression for H:

$$H=M_A^2 p_B+TrP/2+P_{xx}+\left[P_{xy}B_y+P_{xz}B_z\right]/B_x \tag{A9}$$

Under gyrotropic conditions (A9) reduces to (A7). As before, the ion pressure terms in (A9) are those obtained after correction by the factor k_p.

The pressure tensor components needed in the above expressions are given in Table 1, except that the ion terms in (A9) are those already corrected by k_p and that the M_A values are those in Table 2.The resulting net heat flux factors are also in the latter table.

Appendix B: Entropy

In this appendix, we present a brief derivation and discussion of equation (10) and of the associated expression for entropy. For simplicity, we assume that Ohm's law in its simplest form, $\mathbf{E}+(\mathbf{V}\times\mathbf{B})=0$, is valid so that the flow, assumed to be steady and gyrotropic, is exactly field aligned as seen in the HT frame. In this frame, the flow velocity is denoted by $\mathbf{V}'$ and the electric field is zero, $\mathbf{E}'=0$. Under these assumptions, the equation for the conservation of total energy, expressed in the HT frame, takes on a particularly simple form (because the Poynting vector is zero). It becomes an expression for the conservation of total enthalpy:

$$\rho V_x'(\mathrm{d}/\mathrm{d}x)\left(V'^2/2+(3/2)p_{\|}/\rho+p_{\perp}/\rho\right)+\mathrm{d}q_x/\mathrm{d}x=0 \tag{B1}$$

As before, x is a coordinate along the vector normal to the discontinuity surface and q_x is the heat flux along x. The heat flux term may either represent an actual heat flux or it may simply be a catch-all term that accounts for effects, excluded by our model assumptions. The integrated version of this equation becomes equation (A6). Here we will subtract out the rate of mechanical work from (B1) in order to arrive at an expression for entropy. The rate of mechanical work is obtained as the scalar product of the momentum equation with the velocity $\mathbf{V}'$. Since the flow is field aligned, the term $\mathbf{V}'\cdot(\mathbf{J}\times\mathbf{B})$ in the momentum equation will disappear, leaving

$$\nabla\cdot\left(\rho\mathbf{V}'V'^2/2\right)+\mathbf{V}'\cdot\nabla\cdot P=0 \tag{B2}$$

where the pressure tensor, in dyadic notation, is $P=p_{\perp}I+\alpha\mathbf{BB}/\mu_0$. In our one-dimensional geometry we then find

$$\nabla\cdot P=(\mathrm{d}/\mathrm{d}x)\left[P_{xx};P_{xy};P_{xz}\right] \tag{B3}$$

The needed components of the pressure tensor are

$$P_{xx}=p_{\perp}+\alpha B_x^2/\mu_0;P_{xy}=\alpha B_x B_y/\mu_0;P_{xz}=\alpha B_x B_z/\mu_0 \tag{B4}$$

where, as before, $\alpha = \left(p_{\parallel} - p_{\perp}\right)\mu_0/B^2$. Using these expressions, we find

$$\mathbf{V}' \cdot (\nabla \cdot \mathrm{P}) = V_x' \mathrm{d}\left(p_{\perp} + \alpha B_x^2/\mu_0\right)/\mathrm{d}x + V_y' (\mathrm{d}/\mathrm{d}x)\left(\alpha B_x B_y/\mu_0\right) + V_z' (\mathrm{d}/\mathrm{d}x)\left(\alpha B_x B_z/\mu_0\right) \tag{B5}$$

In (B5) we also have $V_y' = V_x'\left(B_y/B_x\right)$ and $V_z' = V_x'\left(B_z/B_x\right)$, since the flow is field aligned. Because B_x is constant, we can then simplify (B5) to give

$$\mathbf{V}' \cdot (\nabla \cdot \mathrm{P}) = V_x' \mathrm{d}p_{\parallel}/\mathrm{d}x - \left(\alpha/2\mu_0\right)\mathrm{d}B^2/\mathrm{d}x \tag{B6}$$

Therefore, the conservation of mechanical energy becomes

$$\rho V_x' (\mathrm{d}/\mathrm{d}x) V'^2/2 = -V_x' \mathrm{d}p_{\parallel}/\mathrm{d}x + V_x'\left(p_{\parallel} - p_{\perp}\right)(\mathrm{d}/\mathrm{d}x)\ln B \tag{B7}$$

If we now eliminate the kinetic energy term from (B1) by use of (B7), and also divide by the constant mass flux, $\rho V_x'$, we find

$$(1/\rho)\left[-\mathrm{d}p_{\parallel}/\mathrm{d}x + \left(p_{\parallel} - p_{\perp}\right)(\mathrm{d}/\mathrm{d}x)\ln B\right] + (\mathrm{d}/\mathrm{d}x)\left(3p_{\parallel}/2\rho + p_{\perp}/\rho\right) + \mathrm{d}\left(q_x/\rho V_x'\right)/\mathrm{d}x = 0 \tag{B8}$$

We can sort this expression into those terms that contain $p_{\parallel}$ and those that contain $p_{\perp}$. The result is

$$p_{\parallel}(\mathrm{d}/\mathrm{d}x)\ln\left(p_{\parallel}B^2/\rho^3\right) + 2p_{\perp}(\mathrm{d}/\mathrm{d}x)\ln\left(p_{\perp}/\rho B\right) + \left(1/V_x'\right)\mathrm{d}q_x/\mathrm{d}x = 0 \tag{B9}$$

In this expression, we recognize the so-called "double-adiabatic invariants" $C_{\parallel} = p_{\parallel}B^2/\rho^3$ and $C_{\perp} = p_{\perp}/\rho B$. Therefore, we can write

$$p_{\parallel}(\mathrm{d}/\mathrm{d}x)\ln C_{\parallel} + 2p_{\perp}(\mathrm{d}/\mathrm{d}x)\ln C_{\perp} + \left(1/V_x'\right)\mathrm{d}q_x/\mathrm{d}x = 0 \tag{B10}$$

To understand the meaning of (B10), we divide it by the factor 2ρ and then use $p_{\parallel} = \rho \mathrm{R} T_{\parallel}$ and $p_{\perp} = \rho \mathrm{R} T_{\perp}$, where $\mathrm{R} = \kappa_b/m_{\mathrm{eff}}$ is the gas constant. We also have $c_{v\parallel} = \mathrm{R}/(\gamma_{\parallel} - 1)$, with $\gamma_{\parallel} = 3$, and $c_{v\perp} = \mathrm{R}/(\gamma_{\perp} - 1)$, with $\gamma_{\perp} = 2$. Here $\gamma = c_p/c_v = (d_f + 2)/d_f$ is the ratio of specific heats at constant pressure and constant volume. The symbol d_f denotes the number of degrees of freedom of the particle motion so that $d_f = 1$ for the motion along the magnetic field and $d_f = 2$ for the motion perpendicular to the magnetic field. Therefore, we find $c_{v\parallel} = \mathrm{R}/2$ and $c_{v\perp} = \mathrm{R}$. With these expressions, equation (B10) can be written in terms of the temperatures as

$$T_{\parallel} c_{v\parallel} \mathrm{d}\ln C_{\parallel}/\mathrm{d}x + T_{\perp} c_{v\perp} \mathrm{d}\ln C_{\perp}/\mathrm{d}x + \left(1/\left(2\rho V_x'\right)\right)\mathrm{d}q_x = 0 \tag{B11}$$

which is equivalent to (10) in the main text.

For consistency, we can also express the parallel and perpendicular invariants as $C_{\parallel} = \kappa_b T (B/N)^2$ and $C_{\perp} = \kappa_b T/B$. Use of the number density, N, instead of mass density $\rho = N m_{\mathrm{eff}}$, is consistent with our assumption that the effective ion mass, although different for the two shocks, is constant within each.

Next, we discuss (B11) as an expression for entropy. By use of the thermodynamic relation, $\mathrm{d}Q = T\mathrm{d}S$, we see that, except for a constant of integration, we can write $S_{\parallel} = c_{v\parallel}\ln C_{\parallel}$ and $S_{\perp} = c_{v\perp}\ln C_{\perp}$ as "partial" entropies so that (B11) can be rewritten as

$$\mathrm{d}Q_{tot}/\mathrm{d}x = \mathrm{d}Q_{\parallel}/\mathrm{d}x + \mathrm{d}Q_{\perp}/\mathrm{d}x + c_{v\parallel}\mathrm{d}\left(q_x/\left(\rho V_x'\right)\right)/\mathrm{d}x = 0 \tag{B12}$$

In effect, the plasma has two energy reservoirs, one for parallel and one for perpendicular motion. Energy can be transferred between these two reservoirs. Energy exchange between neighboring fluid elements can also occur via heat conduction. Because of our assumptions, no internal generation of heat by resistive or viscous effects is explicitly described but any such effects contained in the measured data would manifest themselves in the heat flux term. If there is no such term, it follows that $\mathrm{d}Q_{\mathrm{tot}}/\mathrm{d}x = 0$.

These results indicate that the total entropy can be written as

$$S = S_{\parallel} + S_{\perp} = c_{v\parallel} \ln C_{\parallel} + c_{v\perp} \ln C_{\perp} + \text{const.} = \mathrm{R} \ln \left(C_{\parallel}^{1/2} C_{\perp} \right) + \text{const.} \tag{B13}$$

By use of the expressions for $C_{\parallel}$ and $C_{\perp}$, we can therefore write

$$S = (3\mathrm{R}/2) \ln \left(T_{\parallel}^{1/3} T_{\perp}^{2/3} / N^{2/3} \right) + \text{const.} = (3\mathrm{R}/2) \ln \left(p_{\parallel}^{1/3} p_{\perp}^{2/3} / \rho^{5/3} \right) + \text{const.} \tag{B14}$$

Note that S is a purely thermodynamic state variable: it does not contain the magnetic field. For the special case where $T_{\parallel} = T_{\perp}$, equation (B14) reduces to the usual expression for a monoatomic gas ($\gamma = 5/3$), namely, $S = c_v \ln \left(T/N^{\gamma-1} \right) + \text{const} = c_v \ln \left(p/\rho^{5/3} \right) + \text{const}$.

From the above development, we can draw the following general conclusions for a gyrotropic MHD discontinuity in which resistive and viscous dissipation, as well as any effects produced by electric fields and heat flux, are absent.

1. Either $C_{\parallel}$ and $C_{\perp}$ are both conserved or neither is conserved.
2. If $C_{\parallel}$ and $C_{\perp}$ are both conserved, then the total entropy, given by (B14), is also conserved; if neither is conserved, the total entropy may, or may not, be conserved. If it is not conserved, one would expect it to increase in the flow direction.
3. If $C_{\parallel}$ and $C_{\perp}$ are not conserved, then the variations of the two first terms on the left in (B11) must be anticorrelated so that their sum can remain zero. Deviation from this behavior in an actual event is an indication that one or more of the base assumptions of nonresistive behavior, nonviscous gyrotropic flow, no electric field (in the HT frame), and no heat flux must be violated.
4. In (B11), or (10) in the main text, only the heat flux term is written out explicitly. Any other nonideal behavior present in the shocks would masquerade as a nonzero value of that term.

The mathematical development presented above is by no means new. Except for the heat flux term, equation (B10), or equivalent forms of it, can be found in various textbooks [e.g., *Parks*, 1991, p. 270; *Baumjohann and Treumann*, 1996, p. 137]. In those books and elsewhere, the next step beyond (B10), but with $q_x = 0$, has been to argue that the average magnetic moment, which is in effect proportional to the transverse invariant $C_{\perp}$, should be conserved. From (B10) it then follows that the longitudinal invariant $C_{\parallel}$ must be conserved as well. In our application, we are forced to abandon the assumption that the average magnetic moment, at least as expressed via $C_{\perp}$, is conserved. The reason for the observed behavior could be the presence of counter-streaming populations.

Acknowledgments

The research reported here is part of an International Team effort supported by the International Space Science Institute (ISSI), Bern, Switzerland. We thank the THEMIS team for providing well-calibrated plasma and field data. The individual research efforts were sponsored by NASA under grant NNX12AH43G to the University of Colorado, Boulder (B.S. and S.E) and by grant NNX08AO83G to the University of California, Berkeley, (T.P.). S.H. was supported by the Norwegian Research Council under grant BCSS223252 and DLR under grant 50OC1401. G.P. had support in the form of guest status at MPE, Garching. The data analysis made use of the QSAS science analysis system, provided by Imperial College, London, and available at www.sp.ph.ic..ac.uk/csc-web/QSAS.

References

Auster, H. U., et al. (2008), The THEMIS fluxgate magnetometer, *Space Sci. Rev.*, *141*, 235–264, doi:10.1007/s11214-008-9365-9.

Baumjohann, W., and R. A. Treumann (1996), *Basic Space Plasma Physics*, Imperial College Press, London.

Chew, G. F., M. L. Goldberger, and F. E. Low (1956), The Boltzmann equation and the one-fluid hydromagnetic equations in the absence of particle collisions, *Proc. R. Soc. London, Ser. A*, *236*, 112–118.

McFadden, J. P., C. W. Carlson, D. Larson, M. Ludlam, R. Abiad, B. Elliott, P. Turin, M. Marckwordt, and V. Angelopoulos (2008), The THEMIS ESA plasma instrument and in-flight calibration, *Space Sci. Rev.*, *141*, 277–302.

Parks, G. K. (1991), *Physics of Space Plasmas*, Addison-Wesley Publ. Co., Redwood City, Calif.

Paschmann, G., A. N. Fazakerley, and S. J. Schwartz (1998), Moments of plasma velocity distributions, *ISSI Scientific Reports Series*, *1*, 125–158.

Paschmann, G., I. Papamastorakis, W. Baumjohann, N. Sckopke, C. W. Carlson, B. U. Ö. Sonnerup, and H. Lühr (1986), The magnetopause for large magnetic shear—AMPTE/IRM observations, *J. Geophys. Res.*, *91*, 11,099–11,115, doi:10.1029/JA091iA10p11099.

Sonnerup, B., G. Paschmann, S. Haaland, T. Phan, and S. Eriksson (2016), Reconnection layer bounded by switch-off shocks: Dayside magnetopause crossing by THEMIS D, *J. Geophys. Res. Space Physics*, *121*, 3310–3332, doi:10.1002/2016JA022362.